JOURNAL OF NANO- AND ELECTRONIC PHYSICS
Vol. **10** No 6, 06044(7pp) (2018)

ЖУРНАЛ НАНО- ТА ЕЛЕКТРОННОЇ ФІЗИКИ
Том **10** № 6, 06044(7cc) (2018)

Electronic Structure and X-Ray Photoelectron Spectra of Some Perovskite Molecular Crystals

A.A. Dotsenko[1], O.L. Shcheka[2,*], V.V. Korochentsev[1], A.A. Komissarov[1], V.A. Yashin[1], V.I. Vovna[1]

[1] *Far Eastern Federal University, Vladivostok, Russia*
[2] *Far Eastern State Technical Fisheries University, Russia*

(Received 22 May 2018; revised manuscript received 03 December 2018; published online 18 December 2018)

It is new study of some molecular crystals with a perovskite structure, whose luminescent, thermochromic, nonlinear optical and dielectric properties provide opportunities for their wide practical application. This paper presents the results of an investigation of the electronic structure and the orbital nature of crystals with the AMX_6 formula (where A = Cs, HGu; M = Te, Sb, Ir, Os, Re, W; X = F, Cl, Br). The electronic structure of crystals with Te and Sb atoms was determined by the method of X-ray photoelectron spectroscopy and quantum-chemical modeling within the framework of the density functional theory. We identified the molecular orbitals which are responsible for covalent metal-halogen binding. Also we found that the transition from the $3a_{1g}$ highest occupied molecular orbital to the $4t_{1u}$ lowest unoccupied molecular orbital, which corresponds to the states $^1T_{1u}$ and $^3T_{1u}$, is responsible for the luminescence of the $[MX_6]^{2-}$ anions.

Keywords: Perovskite crystals, s^2-ions, XPS, Density functional theory, Electronic structure, Halides, Luminescence, Molecular orbital.

DOI: 10.21272/jnep.10(6).06044 PACS numbers: 71.15.Mb, 82.80.Pv

1. INTRODUCTION

Molecular crystals with perovskite structure based on s^2-ions (In^+, Tl^+, Ga^+, Pb^{2+}, Bi^{3+}, Te^{4+}, As^{3+}, Sb^{3+} and etc) are of great interest in terms of their application for quantum electronics devices and modern energy sources [1]. It is known that these crystals possess luminescent, thermochromic and nonlinear optical as well as dielectric properties, which makes it possible to use them in mesoscopic solar cells, hole conductors, double-perovskite semiconductors, ferroelectric ceramics with perovskite structure [2, 3]. A huge interest in this class of crystals in recent years is due to the discovery of ferroelectric, ferroelectric and ferroelastic phases [4-6].

These crystals have not only covalent bonds but ionic and metallic ones that contribute to the fact that the total electron density becomes more asymmetric and, as a consequence, shifts to the anion-forming agent. In this case, a larger range is observed between the maximum and minimum value of the periodic potential in the crystal field [7]. Binding to cations the perovskites form clusters with tight packing of layers, where some of them demonstrate polymorphism and phase transitions caused by the dynamics of rotation of organic cations. However, luminescent properties are not observed in certain crystals where halogen ligands F, Cl, Br, I are bound to s^2-ions or metals (it is known that these properties are mostly determined by metal ions with mercury-like electron configuration ns^2). The transitions between sp-excited ^3P_j and s^2-ground $^1S_0$ states are considered responsible for the luminescence process, so luminescence has an intraionic character [8]. An important role in luminescence is also played by the correlation of the Jahn-Teller effect with the spin-orbit interaction, and the presence of an anomalously large Stokes shift, which can reach 20.000 cm^{-1}-30.000 cm^{-1}. The probability of optical transitions in crystals depends mainly on the nearest surroundings of the s^2-ion and its structure. In this case, the unshared electron pair, due to the spin-orbit interaction, leads to mixing the electronic transitions of various types, which further complicates their interpretation.

It is necessary to note that the existing luminescence theory based on the terms of atomic $^1S_0$ and $^1P_1$, ^3P_j states is applicable only for metal ions with s^2- configuration and for describing the luminescence of metal halide anions such as SbX_6^{3-} and TeX_6^{2-} (X = Cl, Br). This applicability is limited by the fact that the 5s-AOs of the metal are hybridized with the group orbitals of halogens, and the rules for selecting optical transitions and localizing electronic states require the use of descriptions in terms of irreducible representations.

All above mentioned requires for a detailed study of the electronic structure of crystals with the ABX_6 general formula (A = Cs, guanidine, N'N-diphenylguanidine; M = Te, Sb, Ir, Os, Re, W; X = F, Cl, Br) in order to determine their physical and chemical properties and sequence of the electronic levels, as well as the definition of the correlation "electronic structure - properties."

2. CALCULATION AND EXPERIMENTAL METHODS

The crystals with Te and Sb atoms studied in this paper were synthesized in the Laboratory of Light-Transforming Materials of the Institute of Chemistry, Far-Eastern Branch of the Russian Academy of Sciences. Synthesis and crystal structure were described in details in the paper [8]. An information about structure of molecular crystals was taken from the paper [9] and Cambridge Structural Data Base [10].

* shcheka37@mail.ru

A great contribution to the understanding of the electronic structure of MF_6 (M = Te, Cr, Mo, W) and identification of the photoelectron spectra was made by calculations [11, 12].

X-ray photoelectron spectra were obtained by us on an Omicron ultrahigh-vacuum photoelectron spectrometer. An X-ray tube with a magnesium anode (MgKα – 1253.6 eV) was used as a source of radiation. The chamber pressure during the experiment did not exceed 9×10^{-9} mbar. The value of the emission current was $I = 13$ mA and the anode voltage – $U = 10$ kV. Sections of the spectra of the characteristic levels of the atoms O1s, C1s, N1s, Cl2p, Br3p were recorded at the transmission energy of the analyzer of 20 eV.

During the registration of spectra the characteristics of the lines did not change. The calibration of the electron binding energy scale was performed based on carbon level C1s. The spectra were processed with the use of Casa XPS software [13]. The test compounds were powders applied to an adhesive substrate.

The spectra were processed by standard procedures. The spectrum background was subtracted by the Shirley method [14]. Spectral smoothing was performed with the use of the Savitzky-Golay digital polynomial filter (SG), a quadratic function with an approximation of interval lenth of 13 points was choosen as a polynomial approximation in the SG filter. The spectra of outer-shell electrons were interpreted on the basis of calculations of the electronic structures of model compounds and regularities in the X-Ray photoelectron spectra of investigated and related compounds according to the procedure we described in [15, 16].

The calculation of the electronic structure was performed by an ab initio quantum chemical method of DFT with the use of the software systems FireFly and GAMESS-US [17, 18] and a hybrid three-paremeter exchange correlation functional B3LYP [19] with effective core potential of R. Ahlrichs for the atoms of tellurium, antimony and cesium [20]. We used the 6-31G, def2-SVP, def2-TZVP basis sets for the calculations [20].

3. RESULTS AND DISCUSSION

3.1 Model Complexes and Electronic Configuration

Figure 1 shows the images of model complexes with the AMX_6 general formula (A = Cs, guanidine, N'N-diphenylguanidine; M = Te, Sb, Ir, Os, Re, W; X = F, Cl, Br).

According to the obtained crystallographic data [9], the complex molecular crystals are anions with the MX_6^z general formula (Fig. 1a), where M = Sb, Te; X = Cl, Br; z – is the charge of the anion, which is surrounded by outer-sphere cations of guanidine (Figure 2b), N'N-diphenylguanidine (Figure 2c) and cesium.

The description of the electronic structure and X-Ray photoelectron spectra of the valence band was carried out on the basis of theoretical modeling in the cluster approximation using model compounds with the MX_6^z general formula and compounds (Fig. 2) taking into account the maximum number of interactions in real crystals.

According to calculation the electronic configuration of the valence band of octahedral anions is:
$1a_{1g}^2 1t_{1u}^6 1e_g^4 2a_{1g}^2 2t_{1u}^6 1t_{2g}^6 2e_g^4 3t_{1u}^6 1t_{2u}^6 1t_{1g}^6 3a_{1g}^2 4t_{1u}^0$.

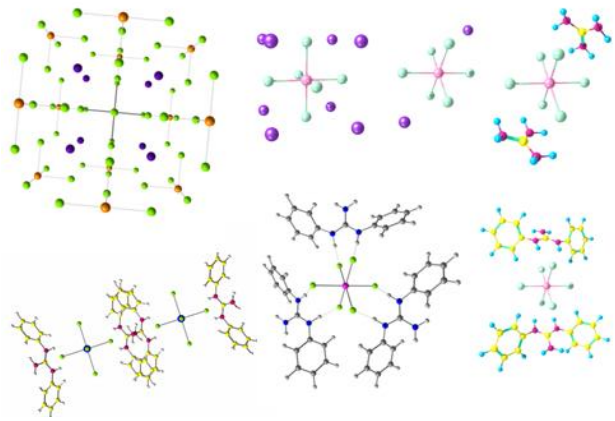

Fig. 1 – Model complexes

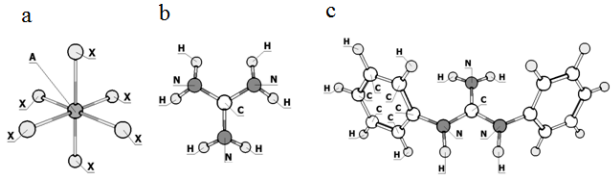

Fig. 2 – The structure of the main fragments of a) anions and cations b) of guanidine, c) N'N-diphenylguanidine in complex molecular crystals

The shape and symmetry of the main molecular orbitals of octahedral anions are shown in Fig. 3 using the example of $[TeCl_6]^{2-}$.

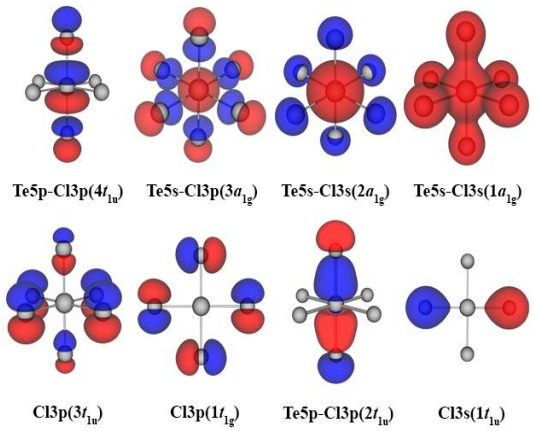

Fig. 3 – The shape and symmetry of the main MOs of anion $[TeCl_6]^{2-}$

3.2 Electronic Structure of Some Perovskite Fluorides

It was previously believed, that LUMO (lowest unoccupied molecular orbital) in these salts is s-type metal valence orbital (its composition according to calculation: 67 % Se 4*s* in SeF_6, 67 % Te 5*s* in TeF_6, 68 % Te 5*s* in TeF_7^- and 63 % Te 5*s* in $OTeF_5^-$), which is antibinding to ligands and corresponding to a stereochemically inactive unshared pair.

The energy of LUMO is extremely sensitive to the lengths of the M-F bonds. Minor changes in distance lead to significant changes in the energy of LUMO. HOMO (highest occupied molecular orbital) in SeF_6, TeF_6 and TeF_7^- is the orbital of the fluorine unshared pair. Removal of one fluorine ligand (Fig. 4) leads to the re-hybridization of the $3a_{1g}$ orbital in TeF_6^{2-} into the $6a_1$ orbital (unshared pair) in TeF_5^-, causing the increase of the length of all Te-F bonds to 2.10 Å. SCF (self-consistent field) calculation demonstrated that in contrast to the heavier halides $[TeX_6]^{2-}$ (where X = Cl, Br), the electron pair $5s^2$ in $[TeF_6]^{2-}$ and $[SeF_6]^{2-}$ can not be easily adapted in a stable octahedral O_h or non-octahedral C_{3u} configuration, and attempts to synthesize salts of $A_2[TeF_6]$ or $A_2[SeF_6]$ types must take into account that these salts can only be stable in solution with a reducing medium and at a low temperature.

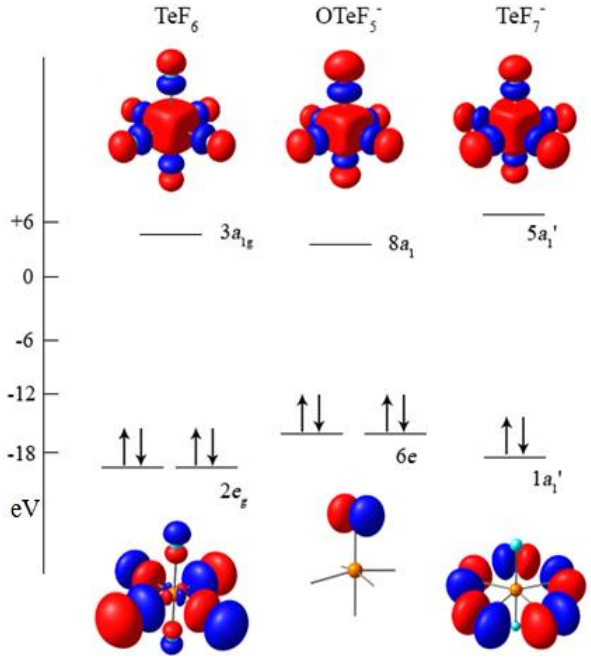

Fig. 4 – Correlation diagram for TeF_6, $OTeF_5^-$, TeF_7^-

Figure 5 shows the one-electron energy of the $(F_6^-)^{6+}$ cluster with the "tie" of the HOMO t_{1g} to the corresponding level in the molecule MoF_6. The energy of MOs of isoelectronic molecules of the TeF_6 type is determined mainly by three factors: a) the energy of atomic orbitals; b) the degree of delocalization of ligand MOs to a central atom; c) the efficiency of the interaction of electron pairs of neighboring halogen atoms, which depends on the interatomic distances.

Covalent bonding in hexahalides of *p*-elements is realized by the interaction of the *ns*- and *np*-orbitals of the central atom with the group $2p_\sigma$- orbitals $a_{1g}(\sigma)$ and $t_{1g}(\sigma)$. The calculation shows the stabilization of the binding orbitals $2a_{1g}$ and $2t_{2g}$ relative to the cluster levels on 5.2 and 3.4 eV. The energy of these two MOs strictly depends on the energy of the 5*s* and 5*p* atomic orbitals of tellurium. The correlation diagram (Fig. 5) shows a slight (~ 1 eV) covalent stabilization of only $2e_g$-MO where the contribution of Te *d*-AO is 10 % according to calculation.

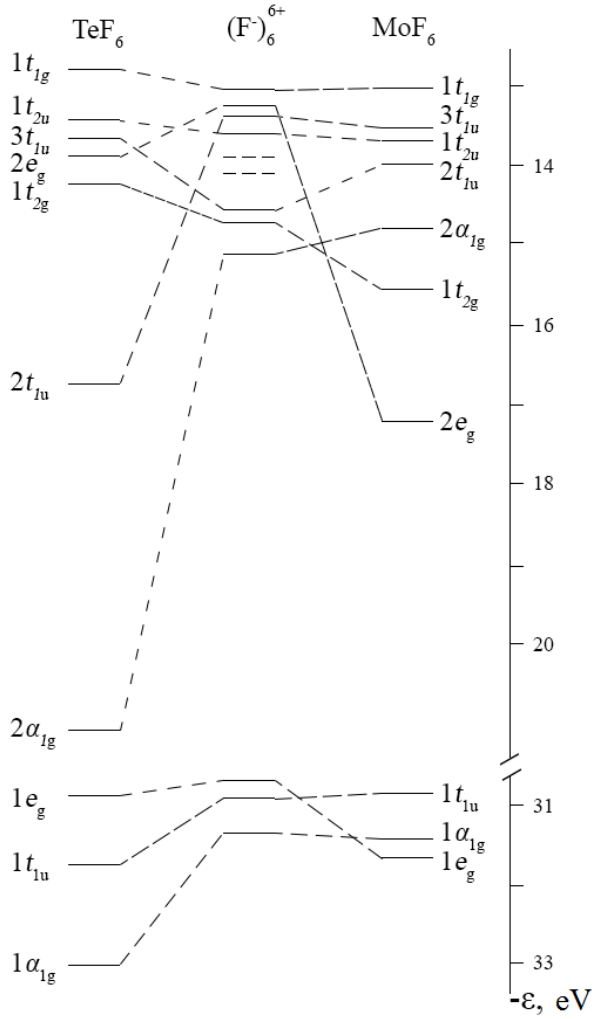

Fig. 5 – Correlation diagram of TeF_6 and MoF_6 orbital energies and $(F_6^-)^{6+}$ group orbital energies

When a *p*-element is replaced by a *d*-metal, the sequence and binding character of the MOs is significantly altered. The orbitals $a_{1g}(\sigma)$ and $t_{1g}(\sigma)$ become practically non-bonding, since their energies are close to the energies of the group orbitals in the cluster, and the orbitals $2e_g$ and $1t_{2g}$ lower the energy by 4.0 and 1.4 eV as a result of mixing with Mo 4d-AO. Fluorine 2*p* – orbitals in octahedral structure are transformed according to irreducible representations t_{1g}, t_{2u}, t_{1u}, t_{2g}, and $2p_\sigma$ -orbitals – to irreducible representations a_{1g}, e_g, t_{1u}. Group orbitals t_{1u}, t_{2g} and a_{1g} are F—F-bonding. Metal atom contributes sufficiently to MOs $2e_g$ and $1t_{2g}$, $2a_{1g}$ and $2t_{1u}$. Fluorine 2*s*-orbitals make remarkable contribution to inner levels $1a_{1g}$, $1t_{1u}$ and $1e_g$.

3.3 XPS Spectra Some Perovskite Fluorides

Six and seven bands in the photoelectron spectra of MF_6 (M = W, Ir, Os, Re) (Fig. 6) are observed respectively in the ionization range of seven p-type orbitals (15-20 eV).

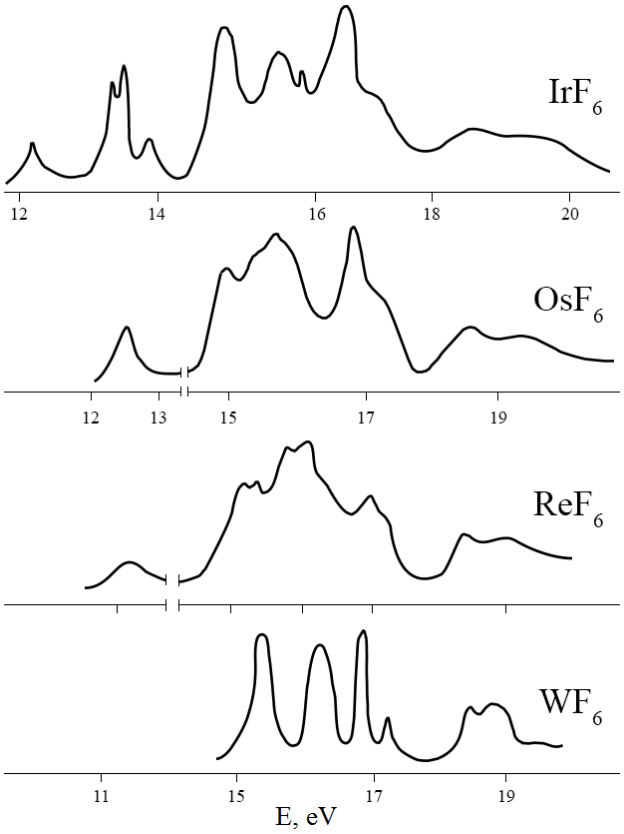

Fig. 6 – Photoelectron spectra of MF_6

According to the calculations (Table 1) the second band in the spectra of both complexes belongs to the levels $1t_{2u}$ and $3t_{1u}$. In WF_6 the additional eighth ionization potential refers to the $2t_{1u}$-level due to the close to the observed spin-orbit splitting obtained. When the spin-orbital interaction is taken into account the triply degenerate MOs split into two sublevels:

$$1t_{1g} \rightarrow \gamma 6g + \gamma 8g;\ 1t_{1u} \rightarrow \gamma 6u + \gamma 8u;$$
$$1t_{2g} \rightarrow \gamma 7g + \gamma 8g;\ 1t_{2u} \rightarrow \gamma 7u + \gamma 8u.$$

The magnitude of the splitting of the γ-levels is directly proportional to the contribution of the p- and d-states of the metal, since the splitting of the F2p-orbitals can be neglected. And the splitting of the t_{2g} -level can be caused by the d-state, and the t_{1u}-level – by the p-state of the metal. For WF_6, the splitting values (eV) are $1t_{2g}$ – 0,15; $2t_{1u}$ – 0,3; $3t_{1u}$ – 0,2.

The relatively large splitting of the ligand levels of t_{1u} symmetry indicates the contribution of the occupied 5p metal orbital, for which the magnitude of the spin-orbital splitting reaches 10 eV. Consequently, the bands in the WF_6 spectrum at 16.83 and 17.22 eV, which have close Frank-Condon contours and the integral ratio of 2:1, in accordance with the calculation can be attributed to the sublevels $\gamma 8u$ and $\gamma 6u$ of orbital $2t_{1u}$.

The contribution of the 5p-orbital is estimated at 4 % from the splitting value (0.41 eV). In the band related to $1t_{2g}$ -orbital of WF_6 we can see two vibrational progressions of valence vibrations υ_1, which confirms the splitting of the binding $1t_{2g}$-orbital due to Md-F2p mixing (Fig. 7).

Obviously, for the MoF_6 molecule there is a contribution of the atomic 4p and 4d orbitals to the MOs of t_{1u} and t_{2g}-symmetry, respectively. In the molecules of following the tungsten elements – Re, Os and Ir – the anti-binding 2t-orbital is occupied.

The single $2t_{2g}$- electron in ReF_6 gives a weak band at 11.43 eV. The removal of one of the two $2t_{2g}$ -electrons in OsF_6 leads to the $G_{3/2}$ and $E_{5/2}$ states (12.50 and 13.10 eV) with a relative population of ~ 6:1. The $2t_{2g}$ configuration in the IrF_6^+ ion gives the $^3T_1$ state as the lowest that is split due to the spin-orbital interaction to states:

$$A_{1g} + E_g + T_{1g} + T_{2g},$$

which follow from the direct multiplication of irreducible representations of the spatial (T_{1g}) and spin (T_{1g}) functions in the double point symmetry group O_h. Four bands of different intensities correspond to these states in the photoelectron spectrum of IrF_6 in the range of 13.3-13.9 eV.

Table 1 – Vertical ionization potentials (eV) for hexafluorides of Mo, W, Re, Os, Ir

MO	MoF_6		WF_6		ReF_6		OsF_6		IrF_6	
	I_a	I_b	I_a	I_b	I_a	I_b	I_a	I_b	I_a	I_b
$2t_{2g}$					11.0	11.43	12.0	12.50 13.10		13.31 (E) 13.40 (T_1) 13.65 (A_1) 13.75 (T_2)
$1t_{1g}$	14.7	15.07	15.1	15.35	14.6	15.10 15.30	14.5	14.91 15.04	14.6	14.8
$1t_{2u}$, $3t_{1u}$	15.05	15.80	15.8	16.07	15.4	15.77 16.1 16.5	15.2	15.52 15.73 15.9		15.5 15.6 15.7
$2t_{1u}$, υ_{8u} υ_{6u}	16.55 16.68	16.55 16.68	16.83 17.22	16.83 17.22	16.8	16.97 17.2	16.6	16.80 17.20		16.6 17.02
$2a_{1g}$	17.62	17.62		18.43	18.0	18.40	17.9	18.52	18.1	18.5
$1t_{2g}$	18.12	18.53	18.4	18.81		18.9		19.3		19.5
$2e_g$	18.93	19.08	19.28	19.36		19.3		19.7		20.1

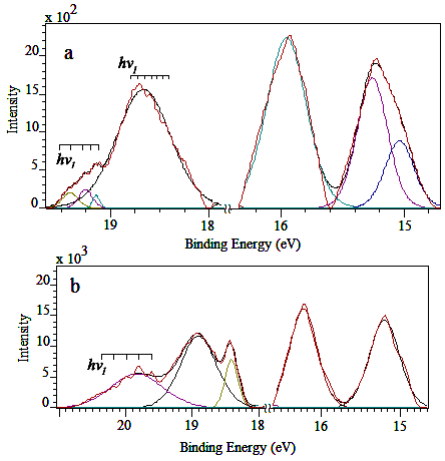

Fig. 7 – Vibration structure of the photoelectron bands for WF_6 (a) and MoF_6 (b)

The energy splitting of the E_g and T_{2g} states (degenerated in the octahedron) indicates a distortion of the octahedron. Unpaired $2t_{2g}$-electrons split ligand levels due to spin polarization. The number of final states for an ion with two unfilled shells can be easily determined from group-theoretical representations.

For example when $1t_{1g}$-electron is removed in ReF_6 the configuration $...1t_{1g}^5 2t_{2g}^1$ leads to ten states if we take into account only the lower state $G_{3/2}$ from the spin-orbital doublet $^2T_{2g} \rightarrow G_{3/2g} + E_{5/2g}$:

$$G_{3/2}(^2T_{1g} \rightarrow G_{3/2g} + E_{1/2g}) = A_{1g} + A_{2g} + {}^2E_g + {}^3T_{2g} + {}^3T_{2g}$$

In X-Ray spectra of MX_6^{n-} ions (M = Ru, Rh, Pd; X = F, Cl; n = 2, 3) [6] the low resolution of the halogen K-lines (Fig. 8) did not allow to determine a sequence of closely related ligand levels.

Table 2 – Orbital energies and contributions of atoms to valence MOs of octahedral anions

$[TeCl_6]^0$				$[TeCl_6]^{2-}$				$[TeBr_6]^0$				$[TeBr_6]^{2-}$			
$-\varepsilon$, eV	MO	Te	X	$-\varepsilon$, eV	MO	Te	X	$-\varepsilon$, eV	MO	Te	X	$-\varepsilon$, eV	MO	Te	X
2,10	$3a_{1g}^2$	–	–	4,26	$3a_{1g}^2$	10	90	3,20	$3a_{1g}^2$	–	–	4,71	$3a_{1g}^2$	7	93
5,00	$1t_{1g}^6$	0	100	5,00	$1t_{1g}^6$	0	100	5,00	$1t_{1g}^6$	0	100	5,00	$1t_{1g}^6$	0	100
5,63	$1t_{2u}^6$	1	99	5,38	$1t_{2u}^6$	0	100	5,60	$1t_{2u}^6$	0	100	5,38	$1t_{2u}^6$	0	100
5,68	$3t_{1u}^6$	4	96	5,42	$3t_{1u}^6$	2	98	5,62	$3t_{1u}^6$	0	100	5,42	$3t_{1u}^6$	0	100
6,34	$2e_g^4$	9	91	5,93	$2e_g^4$	7	93	6,22	$2e_g^4$	11	89	5,87	$2e_g^4$	7	93
6,70	$1t_{2g}^6$	7	93	6,04	$1t_{2g}^6$	3	97	6,57	$1t_{2g}^6$	5	95	6,04	$1t_{2g}^6$	3	97
9,46	$2t_{1u}^6$	34	66	8,30	$2t_{1u}^6$	33	67	9,43	$2t_{1u}^6$	39	61	8,37	$2t_{1u}^6$	37	63
14,72	$2a_{1g}^2$	44	56	14,83	$2a_{1g}^2$	61	39	15,30	$2a_{1g}^2$	44	56	15,30	$2a_{1g}^2$	58	42
18,66	$1e_g^4$	3	97	18,13	$1e_g^4$	2	98	18,15	$1e_g^4$	3	97	17,67	$1e_g^4$	2	98
19,25	$1t_{1u}^6$	9	91	18,37	$1t_{1u}^6$	5	95	18,60	$1t_{1u}^6$	7	93	17,87	$1t_{1u}^6$	5	95
21,39	$1a_{1g}^2$	36	64	19,46	$1a_{1g}^2$	28	72	20,57	$1a_{1g}^2$	41	59	18,98	$1a_{1g}^2$	34	66
$[SbCl_6]^-$				$[SbCl_6]^{3-}$				$[SbBr_6]^-$				$[SbBr_6]^{3-}$			
$-\varepsilon$, eV	MO	Sb	X	$-\varepsilon$, eV	MO	Sb	X	$-\varepsilon$, eV	MO	Sb	X	$-\varepsilon$, eV	MO	Sb	X
3,37	$3a_{1g}^2$	–	–	4,19	$3a_{1g}^2$	16	84	2,63	$3a_{1g}^2$	–	–	4,60	$3a_{1g}^2$	11	89
5,00	$1t_{1g}^6$	0	100	5,00	$1t_{1g}^6$	0	100	5,00	$1t_{1g}^6$	0	100	5,00	$1t_{1g}^6$	0	100
5,49	$1t_{2u}^6$	0	100	5,22	$1t_{2u}^6$	0	100	5,50	$1t_{2u}^6$	0	100	5,25	$1t_{2u}^6$	0	100
5,52	$3t_{1u}^6$	3	97	5,23	$3t_{1u}^6$	1	99	5,51	$3t_{1u}^6$	2	98	5,25	$3t_{1u}^6$	0	100
6,09	$2e_g^4$	7	93	5,63	$2e_g^4$	3	97	6,07	$2e_g^4$	7	93	5,64	$2e_g^4$	3	97
6,39	$1t_{2g}^6$	3	97	5,60	$1t_{2g}^6$	1	99	6,37	$1t_{2g}^6$	3	97	5,68	$1t_{2g}^6$	1	99
8,49	$2t_{1u}^6$	26	74	7,08	$2t_{1u}^6$	27	73	8,49	$2t_{1u}^6$	29	71	7,15	$2t_{1u}^6$	28	72
12,93	$2a_{1g}^2$	49	51	12,48	$2a_{1g}^2$	79	21	13,46	$2a_{1g}^2$	56	44	13,01	$2a_{1g}^2$	80	20
18,36	$1e_g^4$	2	98	17,76	$1e_g^4$	1	99	17,94	$1e_g^4$	2	98	17,37	$1e_g^4$	0	100
18,80	$1t_{1u}^6$	4	96	17,87	$1t_{1u}^6$	2	98	18,27	$1t_{1u}^6$	3	97	17,47	$1t_{1u}^6$	1	99
20,03	$1a_{1g}^2$	19	81	18,23	$1a_{1g}^2$	9	91	19,34	$1a_{1g}^2$	18	82	17,81	$1a_{1g}^2$	9	91

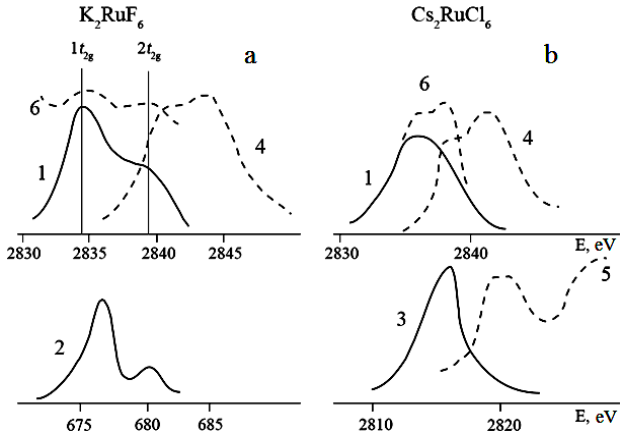

Fig. 8 – Spectra of a) K_2RuF_6 and b) Cs_2RuCl_6, where 1 – Ru $L_{\beta 2}$; 2 – F K_α; 3 – Cl K_α; 4 – Ru L_β – absorption edge; 5 – Cl K - absorption edge; 6 – X-Ray photoelectron spectra

Saving an unchanged sequence $2t_{2g} < 1t_{1g} < 1t_{2u} \sim 3t_{1u} < 2t_{1u} < 2a_{1g} < 1t_{2g} < 2e_g$ in the series of neutral d-element fluorides considered above suggests the same or a similar sequence of levels in the MX_6 ions (M = Sb, Te; X = Cl, Br).

3.4 Electronic Structure of Chlorides and Bromides Anions

The $3a_{1g}$ orbital is unoccupied in the compounds $[TeX_6]^0$, $[SbX_6]^{1-}$, but two additional electrons in $3a_{1g}$ of $[SbCl_6]^{3-}$ cause an increase in the bond length of Sb-Cl from 2.44 Å in $[SbCl_6]^-$ to 2.80 Å as a result of a decrease in the multiplicity of the Sb-Cl bond from 0.255 to 0.115.

A similar regularity is observed for antimony bromides: the multiplicity of the bond decreases from 0.738 to 0.482, the interatomic distances of Sb-Br increase from 2.63 to 2.97 Å. In tellurium compounds, two electrons in $3a_{1g}$ of $[TeCl_6]^{2-}$ cause an increase in the Te-Cl bond length from 2.37 in $[TeCl_6]^0$ to 2.61 Å due to a decrease in the Te-Cl multiplicity of the bond from 0.308 to 0.109. For tellurium bromides the multiplicity of the bond decreases from 0.297 to 0.126, the Te-Br interatomic distances increase from 2.58 to 2.79 Å.

Three lowest MOs $1a_{1g}^2\ 1t_{1u}^6\ 1e_g^4$ of anions $[SbX_6]^-$ and $[SbX_6]^{3-}$ contain the predominant contributions of halogen ns-AOs, but $1a_{1g}$ makes a notable contribution to Sb-X binding due to Sb5s-Xns overlap, where $n = 3$ and 4 respectively for Cl and Br (Table. 2, Fig. 3). Bonding MO $2a_{1g}$ in $[SbX_6]^-$ has close contributions of metal 5*s* AO and Xnp_σ. But in $[SbX_6]^{3-}$ this orbital includes up to 80 % of antimony 5s AO and combination of halogen 3*s* (4*s*) and $3p_\sigma$ ($4p_\sigma$) orbitals. The contributions of np_σ-orbitals enhance the Sb-X binding, and the contributions of the ns orbitals (unlike $1a_{1g}$) are antibonding.

The dominance of *s*-AO in the *s*-p_σ-hybrid orbital of halogen led to the presence of a nodal surface between Sb and X_6 in the MO $2a_{1g}$ (Fig. 3). The main role in the covalent binding of Sb-X is played by 6 electrons of $2t_{1u}$ MO, which realizes the Sb5*p*-Xnp_σ interaction. And 28 electrons of nonbonding MOs $1t_{2g}^6 2e_g^4 3t_{1u}^6 1t_{2u}^6 1t_{1g}^6$, localized on halogen atoms from 97 to 100 %, are important when considering the degree of ionicity of the bonds and the charge transfer process X → Sb in excited states.

According to the calculation the occupied in the anion $[SbX_6]^{3-}$ HOMO $3a_{1g}$ is an antibonding combination of Xnp_σ-orbitals and metal 5*s*-AO (16 % - $[SbCl_6]^{3-}$, 11 % - $[SbBr_6]^-$). When occupying $3a_{1g}$, the structure of $2a_{1g}$ changes markedly: the contribution of tellurium 5s AO increases to 61 % and 58 %, respectively, for compounds with chlorine and bromine, which is represented in the correlation diagram (Fig. 9).

The triply degenerate *t*-MOs of anions, due to the lowering the symmetry, split into:

$$t_{1u} \rightarrow a_{2u} + e_u;\ t_{2g} \rightarrow e_g + a_{1g};\ t_{2u} \rightarrow a_{1u} + e_u;\ t_{1g} \rightarrow a_{2g} + e_g;$$

or into:

$t_{1g} \rightarrow b_g + b_g + a_g$, $t_{2u} \rightarrow b_u + b_u + a_u$, $t_{1u} \rightarrow a_g + a_u + b_u$, $a_u + b_u + b_u$, $b_u + a_g + b_u$ and similarly for e MOs.

At the same time, a relative sequence of electronic levels does not change, analogous to octahedral anions MX_6^z.

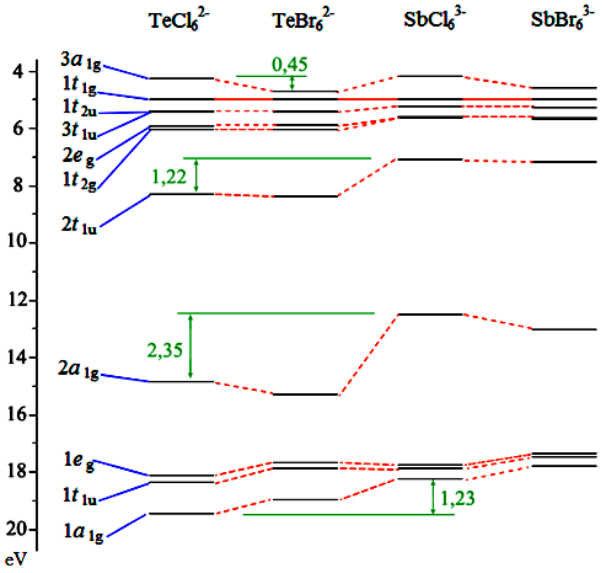

Fig. 9 – The correlation diagram of the MO energies for octahedral anions with the general formula MX_6

3.5 XPS Spectra Valence Bands Perovskite Cs_2TeCl_6

The intense narrow band 1 with maximum at 3.74 eV (Figure 10) in the spectrum of $TeCl_6Cs_2$ is due to a group of non-bonding Xnp-levels of halogens correlating with the MOs $1t_{2g}^6 2e_g^4 3t_{1u}^6\ 1t_{2u}^6 1t_{1g}^6$ of octahedron TeX_6^{2-}. The bend 1′ in the first band at 1.48 eV corresponds to TeX_6^{2-} $3a_{1g}^2$ HOMO.

Band 2 corresponds to the bonding $2t_{1u}^6$ MO (Te5p + halogen Xnp_σ). The bands 3 and 4 are due to the Cs5p MO, and their splitting into two bands is explained by the spin-orbital interaction, which is not taken into account by the DFT method. Band 5 with a maximum at 14.6 eV in X-Ray photoelectron spectrum (Fig. 10) corresponds to the anion MOs $2a_{1g}^2$, $1t_{1u}^6$, $1e_g^4$.

The changes in the intensity and position of the va-

lence-electron bands during the substitution of Cl by Br are due to the fact that binding energy of bromine 4*s* and 4*p* electrons decreases comparing to chlorine 3*s* and 3*p* electrons, and the ionization cross-section of Br4*p* AO increases comparing to Cl3*p* AO.

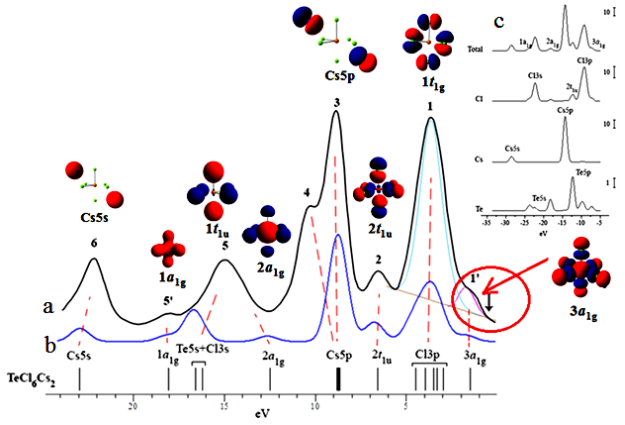

Fig. 10 – Valence bands of X-Ray photoelectron spectrum (a), theoretical spectrum (b) and partial densities (c) for Cs_2TeCl_6

4. CONCLUSION

According to the experimental data and the calculation the $3a_{1g}$ is the HOMO in molecular crystals studied, which is an antibonding combination of Xnp_σ orbitals with a contribution of the halogen atoms of 85 %. Previously this MO was believed to be a metallic nature primarily. It has been determined that in the anions the main role in the covalent metal-halogen binding is played by 6 electrons of $2t_{1u}^6$ MO, and 28 electrons of non-bonding $1t_{2g}^6 2e_g^4 3t_{1u}^6 1t_{2u}^6 1t_{1g}^6$ MOs, localized mainly on halogen atoms. It is essential when considering the degree of ionicity of the bonds and the charge transfer processes in excited states. The transition from the $3a_{1g}$ HOMO to the $4t_{1u}$ LUMO, which corresponds to the states $^1T_{1u}$ and $^3T_{1u}$, is responsible for the luminescence of the $[MX_6]^{2-}$ anions.

AKNOWLEDGEMENTS

The work was supported by the Ministry of Education and Science of the Russian Federation within the framework of project part of the state task (Project No. 3.2168.2017/4.6).

REFERENCES

1. Ze-Ping Wang, Jin-Yun Wang, Jian-Rong Li, Mei-Ling Feng, Guo-Dong Zoua, Xiao-Ying Huang, *Chem. Commun.* **51**, 3094 (2015).
2. A.E. Maughan, A.M. Ganose, M.M. Bordelon, E.M. Miller, D.O. Scanlon, J.R. Neilson, *J. Am. Chem. Soc.* **138** No 27, 8453 (2016).
3. M. Liu, M.B. Johnston, H.J. Snaith, *Nature* **501**, 395 (2013).
4. J. Tarasiewicz, R. Jakubas, J. Zaleski, J. Baran, *J. Mol. Struct.* **876**, 86 (2008).
5. A. Piecha, A. Gagor, A. Pietraszko, R. Jakubas, *J. Solid State Chem.* **183**, 3058 (2010).
6. N. Weslati, I. Chaabane, A. Bulou, F. Hlel, *Physica B* **441**, 42 (2014).
7. R.J.D. Tilley, *Perovskites: Structure-Property Relationships* (UK, London: Wiley: 2016).
8. T.V. Sedakova, A.G. Mirochnik, *Opt. Spectroscop.* **119**, 54 (2015).
9. A. Waskowska, J. Janczak, Z. Czapla, *J. Alloy. Compd.* **196**, 255 (1993).
10. C.R. Groom, I.J. Bruno, M.P .Lightfoot, S.C. Ward, *The Cambridge Structural Database, Acta Crystallographica Section,* **B72**, 171 (2016).
11. J.E. Bloor, H.E. Sherrod, *J. Am. Chem. Soc.* **102**, 4333 (1980).
12. G.L. Gutsev, A.A. Levin, *Chem. Phys*, **51**, 459 (1980).
13. Casa XPS. http://www.casaxps.com/
14. I.N. Levine, *Quantum Chemistry* (New Jersey: Pearson: 2013).
15. A.A. Dotsenko, O.L. Shcheka, V.I. Vovna, V.V. Korochentsev, A.G. Mirochnik, T.V. Sedakova, *J. Mol. Struct.* **1109**, 13 (2016).
16. V.I. Vovna, A.A. Dotsenko, V.V. Korochentsev, O.L. Shcheka, I.S. Os'mushko, A.G. Mirochnik, T.V. Sedakova, V.I. Sergienko, *J. Mol. Struct.* **1091**, 138 (2015).
17. M.S. Gordon, M.W. Schmidt, *Theory and Applications of Computational Chemistry: the first forty years* (Ed. C.E.Dykstra, G.Frenking, K.S.Kim, G.E.Scuseria) (Amsterdam: Elsevier: 2005).
18. A.A. Granovsky, *Firefly version 7.1.G.* http://classic.chem.msu.su/gran/firefly/index.html
19. A.D. Becke, *J. Chem. Phys.* **98**, 5648 (1993).
20. *Basis Set Exchange: v1.2.2.* https://bse.pnl.gov/bse/portal